J. Plasma Physics (2003), *vol.* 69, *part* 6, *pp.* 485–506.
DOI: 10.1017/S0022377803002265 Printed in the United Kingdom

The floating potential of spherical probes and dust grains. II: Orbital motion theory

R. V. KENNEDY and J. E. ALLEN

Christ Church, Oxford OX1 1DP, UK and University College, Oxford OX1 4BH, UK
(rodk@eros.net)

(Received 6 January 2003)

Abstract. Probe theory is generally used to find the potential of dust particles immersed in plasma. The orbital motion limited theory (OML) is often used to find the potential at the probe surface, but the assumptions underlying this theory are usually not valid in the case of dust and the more general orbital motion (OM) theory is much harder to calculate. Solutions are given for the OM theory in a range of cases applicable to dust. It is shown that the surface potential the full theory gives reduces to the OML result for small probes. Commonly in dusty plasmas the OML surface potential is used, with the surrounding distribution given by Debye–Hückel, or Yukawa theory. This form, however, neglects ion depletion due to the absorption of particles on the probe surface. In this paper a new analytical solution to the system is given which is applicable to small probes and dust. This new expression is equivalent to Yukawa form, but takes ion absorption into account.

1. Introduction

Dust particles may be found immersed in plasma in space or in the laboratory. Probe theory is generally used to find the potential of these particles. If ions are cold, the radial motion theory can be used, as developed by Allen et al. (1957). The small probe limit of this theory has been examined by Kennedy and Allen (2001). If ion temperature is considered to be finite the purely radial theory is no longer strictly applicable. The simplest orbital theory is orbital motion limited (OML), which gives a surface potential independent of the dust particle's size (Langmuir and Mott-Smith 1926). OML predicts a surface potential without reference to the potential profile outside the probe. However, the form of that profile may be such that the OML potential is not valid. While perhaps the most widely used theory in dusty plasma work, there is evidence that the conditions for OML to be valid are never met in the parameter range of interest. In particular, the assumptions underlying OML theory are usually not valid in the case of dust (Allen et al. 2000). The more general orbital motion (OM) involves solving simultaneously for the surface potential, the potential distribution around the probe, and the distribution of ion trajectories (see Bernstein and Rabinowitz 1959; Laframboise 1966). This theory is much harder to calculate than the radial motion theory or the OML potential. Commonly, instead of a Maxwellian ion velocity distribution, the simpler assumption is made that ions are distributed isotropically with a single kinetic energy. Although Al'Pert et al. (1965) and Laframboise (1966) obtained solutions for Maxwellian ions, the monoenergetic

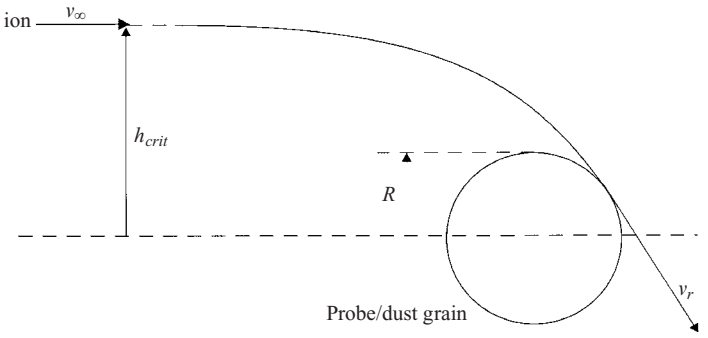

Figure 1. An ion approaching a negatively charged spherical probe from infinity, which just grazes the probe surface.

approach has been much more common (see, for example, Chen 1965; Nowlin and Carlile 1991; or Daugherty et al. 1992). Commonly in dusty plasmas the OML surface potential is used, with the surrounding distribution given by Debye–Hückel or Yukawa theory. This theory provides a distribution of potential calculated from a linearized form of the Poisson equation. This form, however, neglects ion depletion due to the absorption of particles on the probe surface.

In Sec. 2 the OML theory is derived, and it is shown in what circumstances it is valid. In Sec. 3 the Debye–Hückel potential is derived. In Sec. 4 the complete orbital motion theory is described in a new formulation. Results are presented for a wide variety of probe sizes and ion–electron temperature ratios. In Sec. 5 it is shown that a limiting case of this theory exists for small probes. A new linearized expression is given which is equivalent to Yukawa form, but takes into account ion absorption. It is shown that the OML potential is the small probe limit of the result of the full OM theory. Conclusions are drawn in Sec. 6

2. Orbital motion limited

2.1. Theory description

The name refers to the idea that the angular momentum of the ions imposes a limit on the maximum ion current, by analogy with space-charge limited theories. Consider an ion approaching a negatively charged spherical probe from infinity, which just grazes the probe surface, as seen in Fig. 1. Let v_∞ be the velocity at infinity, R be the probe radius, and h be the impact parameter. The critical value of h such that the ion should approach the probe surface tangentially is $h_{\rm crit}$. Conservation of energy E gives

$$E = \tfrac{1}{2}M_{\rm i}v_\infty^2 = \tfrac{1}{2}M_{\rm i}v^2 + eV(r) = \tfrac{1}{2}M_{\rm i}v_R^2 + eV_p \tag{1}$$

where $M_{\rm i}$ is the ion mass, e the electron charge, v is the ion speed, and $V(r)$ the potential at r, v_R the ion speed at R and V_p the surface potential. Conservation of angular momentum J gives

$$J = mv_\infty h. \tag{2}$$

So to graze the probe surface the critical values are:

$$J_{\rm crit} = mv_\infty h_{\rm crit} = mv_R R. \tag{3}$$

https://doi.org/10.1017/S0022377803002265 Published online by Cambridge University Press

Substituting for v_R from (3) into (1),

$$h_{\rm crit} = R\sqrt{1 - \frac{2eV_p}{M_{\rm i}v_\infty^2}} \tag{4}$$

or alternatively,

$$J_{\rm crit} = M_{\rm i}v_\infty R\sqrt{1 - \frac{2eV_p}{M_{\rm i}v_\infty^2}}\,. \tag{5}$$

Assume that any ions with h smaller than $h_{\rm crit}(v_\infty)$ will hit the probe, and that all other ions will miss. The contribution to the ion current from ions with velocity v is thus

$$dI = \begin{cases} -ef(v)u(r)\,d^3v & J \leqslant J_{\rm crit} \\ 0 & J > J_{\rm crit} \end{cases} \tag{6}$$

where $f(v)$ is the ion distribution function, $u(r)$ is the radial velocity at r positive outwards, and r is any radius greater than R. Integrating (6),

$$I_{\rm i} = 4\pi r^2 \int_{J<J_{\rm crit}} ef(v)u(r)\,d^3v. \tag{7}$$

Using (1) and (2) we change variable from v to E and J:

$$d^3v = \frac{2\pi}{M_{\rm i}^2 r^2 u} J\,dJ\,dE \tag{8}$$

where the radial velocity u is, from (1) and (2),

$$u = \sqrt{\frac{2}{M_{\rm i}}(E - eV) - \frac{J^2}{M_{\rm i}^2 r^2}}\,. \tag{9}$$

We perform the integration at arbitrarily large r in order to use the distribution in the plasma, which we assume to be Maxwellian,

$$f_{\rm M}(v) = n_0\left(\frac{M_{\rm i}}{2\pi kT_{\rm i}}\right)^{3/2} \exp\left(-\frac{\frac{1}{2}M_{\rm i}v^2}{kT_{\rm i}}\right) = n_0\left(\frac{M_{\rm i}}{2\pi kT_{\rm i}}\right)^{3/2} \exp\left(-\frac{E}{kT_{\rm i}}\right) \tag{10}$$

where n_0 is the density far from the probe and $T_{\rm i}$ is the ion temperature. Substituting (8) and (10) into (7), and using (5) for the angular momentum limit, we obtain

$$I_{\rm i} = 4\pi R^2 en_0\sqrt{\frac{kT_{\rm i}}{2\pi M_{\rm i}}}\left(1 - \frac{eV_p}{kT_{\rm i}}\right). \tag{11}$$

To obtain the floating potential we let $I_{\rm i} = I_{\rm e}$ and use the electron surface flux (see Kennedy and Allen 2001):

$$I_{\rm e} = 4\pi R^2 n_0 e\sqrt{\frac{kT_{\rm e}}{2\pi m_{\rm e}}} \exp\left(\frac{eV_p}{kT_{\rm e}}\right). \tag{12}$$

So equating (11) and (12),

$$\left(1 + \frac{1}{\beta}\eta_p\right)\exp(\eta_p) = \sqrt{\frac{M_{\rm i}}{m_{\rm e}}}\,\sqrt{\beta} \tag{13}$$

where η_p is the normalized surface potential $-eV_p/kT_{\rm e}$ and β is the ratio of ion to electron temperature $T_{\rm i}/T_{\rm e}$. Note that the dependence on R cancels out and we are

https://doi.org/10.1017/S0022377803002265 Published online by Cambridge University Press

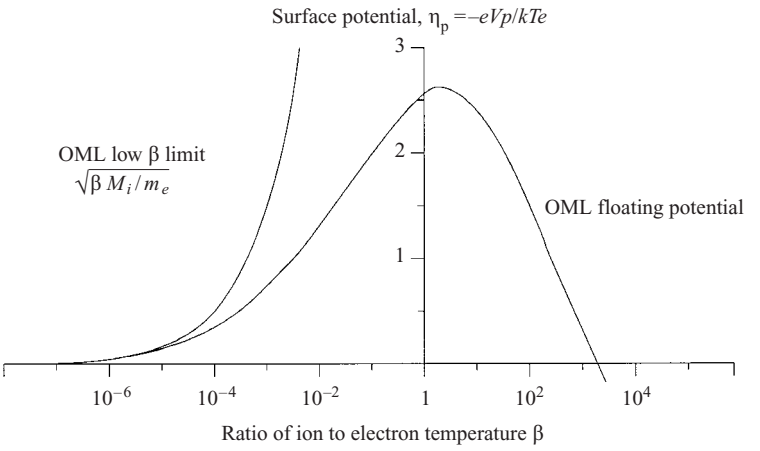

Figure 2. OML solutions for floating potential from (18) plotted against ion–electron temperature ratio β.

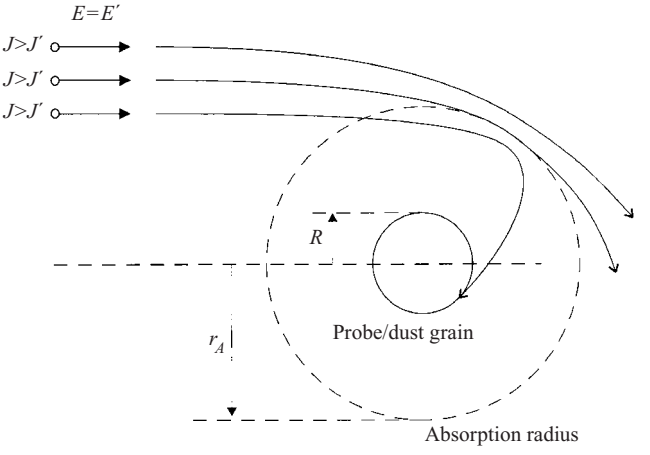

Figure 3. The absorption radius phenomenon. In the situation illustrated, an ion of energy E and angular momentum smaller than J' will always hit the probe. An ion of energy E and larger J will not approach closer than r.

left with a relationship between η_p, β, and mass ratio. Figure 2 shows the results of (13) plotted against a logarithmic scale in β. In laboratory plasmas, it is rare for β to be greater than 0.1, and in general plasmas values greater than unity are not expected. The limit of floating potential as ion temperature tends to zero is itself zero.

2.2. Limitations

There are circumstances when OML is not applicable. Suppose that for a given energy and angular momentum $\{E', J'\}$ at some $r_A > R$ we have $u(r_A) = 0$, as shown in Fig. 3. It follows from (9) that an ion with $\{E', J > J'\}$ has no solution

https://doi.org/10.1017/S0022377803002265 Published online by Cambridge University Press

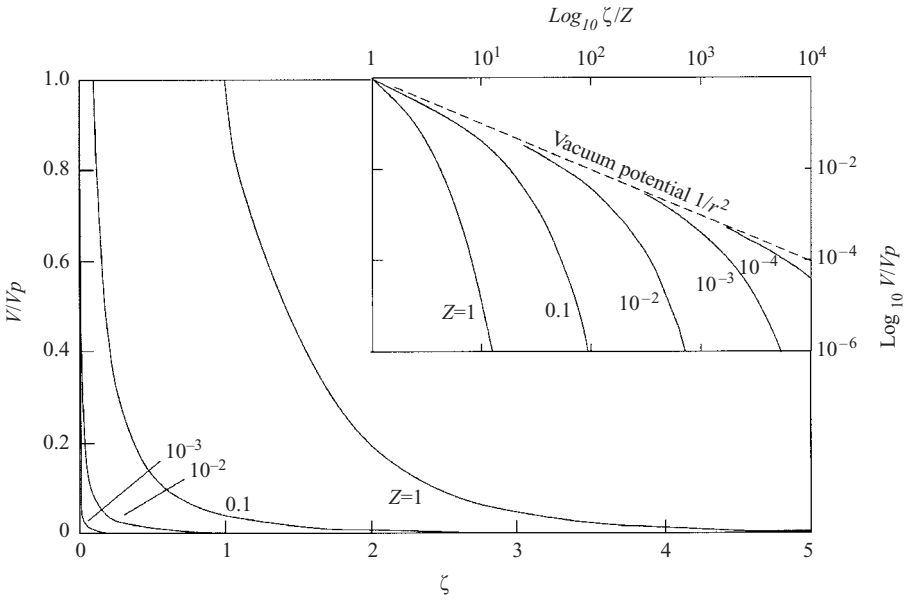

Figure 4. Plots of the Debye–Hückel potential (22) for various values of normalized probe radius Z.

for $u(r)$ at $r = r_A$. From (9) at r_A,

$$E' - eV(r_A) = \frac{J'^2}{2M_i^2 r_A^2}. \tag{14}$$

Suppose also that in the interval $r \in \{R, r_A\}$ for E', J' positive solutions exist for $u(r)$. This situation is illustrated in Fig. 4. Assuming all functions are smoothly varying, an ion with infinitesimally greater angular momentum than J' would be reflected near to r_A, while an ion with infinitesimally smaller angular momentum would strike the probe with finite radial velocity. For no value of J less than J' would an ion of energy E' approach the probe tangentially. So the definition of J_{crit} in (6) and (7) should now no longer be that given by (5). We call r_A an absorption radius (AR) and if it exists, OML cannot be assumed to apply.

DEFINITION. *The absorption radius $r_A(E)$ is the smallest radius an ion with energy E can reach without striking the probe, where such a radius exists.*

For OML to be valid we require $u(r) > 0$ at all $r > R$ for all relevant energies E and all $J < (J_{crit})_{OML}$. It is sufficient to require this for all relevant E and r as follows:

OML valid iff:

$$E - eV(r) > (E - eV_p)\frac{R^2}{r^2}. \tag{15}$$

Note that V is negative. By 'all relevant E' we mean all energies for which the distribution function $f(E)$ is finite. In the case of Maxwellian velocity distributions (15) must be true as $E \to 0$. A necessary and sufficient condition is thus:

https://doi.org/10.1017/S0022377803002265 Published online by Cambridge University Press

where $f = f_M$, OML valid iff:

$$\frac{V(r)}{V_p} > \frac{R^2}{r^2}. \tag{16}$$

The monoenergetic case is less stringent—(15) is used where E is the ion energy. See Sec. 4.2.2 for a rigorous treatment of the case where ARs exist.

3. Debye–Hückel theory

The Debye–Hückel potential is obtained by assuming a known surface potential on the probe, and solving the linearized Poisson equation (Bouchoule 1999). Assuming a Boltzmann relation for electrons

$$n_e(r) = n_0 \exp\left(\frac{eV(r)}{kT_e}\right) \tag{17}$$

and an ion density of the equivalent form

$$n_i(r) = n_0 \exp\left(-\frac{eV(r)}{kT_i}\right), \tag{18}$$

the Poisson equation is

$$\nabla^2 V = \frac{e}{\varepsilon_0}(n_e - n_i). \tag{19}$$

Substituting (17) and (18) into (19) with spherical symmetry, and normalizing,

$$\frac{d^2V}{d\zeta^2} + \frac{2}{\zeta}\frac{dV}{d\zeta} = V \tag{20}$$

where $\zeta = r/\lambda_{DL}$ and λ_{DL} is the linearized Debye length:

$$\frac{1}{\lambda_{DL}^2} = \frac{1}{\lambda_{De}^2} + \frac{1}{\lambda_{Di}^2}; \tag{21}$$

$\lambda_{De} = \sqrt{\varepsilon_0 kT_e/n_0e^2}$ and $\lambda_{Di} = \sqrt{\varepsilon_0 kT_i/n_0e^2}$ are the electron and ion Debye lengths, respectively. The analytical solution to (20) is

$$V = V_p \frac{Z}{\zeta} \exp(Z - \zeta) \tag{22}$$

where $Z = R/\lambda_{DL}$. Figure 4 shows plots of (22) for various values of Z. It is clear from the logarithmic plot in the inset that, as Z becomes smaller, a greater part of the curve follows the vacuum solution $V \propto 1/r^2$ which is a solution to $\nabla^2 V = 0$ in spherical symmetry. This is because, for very small ζ, the two left-hand-side terms of (20) are much larger than V, but of opposite sign, almost exactly cancelling out. For this reason, the error caused by linearizing the right-hand side of the Poisson equation becomes negligible for small Z. Debye–Hückel theory is generally used for probes of small radius compared to the Debye length, such as dust particles. This theory gives no information about equilibrium surface potential.

4. Full orbital motion theory

4.1. Introduction

Langmuir's absorption radius concept was explored further by Bohm et al. (1949), who obtained a solution for monoenergetic ions with an isotropic distribution far

https://doi.org/10.1017/S0022377803002265 Published online by Cambridge University Press

from the probe, in the thin-sheath limit. Bohm et al. used a plasma approximation. Bernstein and Rabinowitz (1959) formulated the complete problem of a spherical probe in a plasma with Maxwellian electrons and ions of arbitrary distribution, with a finite sheath thickness. They obtained the solution for monoenergetic ions.

Al'Pert et al. (1965) and Laframboise (1966) extended this approach, introducing a Maxwellian ion distribution in the plasma. It was found that in this case the absorption radius was no longer a single quantity, but a function of ion energy and that this function had finite values for all energies below a certain level for the parameters they used. Only Laframboise tabulated his results in full, and he did not find many solutions for R/λ_{De} below unity, possibly due to numerical difficulties. This is the parameter range of interest regarding dust.

Allen et al. (2000) have shown that for Maxwellian ions the criterion for having no absorption radius is never met for ion temperatures in the parameter range of interest.

Many authors have foregone the complete analysis and assumed that the linear Debye–Hückel shielded potential is applicable (see, for example, Bouchoule 1999). As this approach assumes ions to be in equilibrium, another method must be used to obtain the floating potential to be used as the initial parameter.

In this section the OM theory will be developed in full for the case of Maxwellian ions, and results given for the floating potential and potential distribution. The results of Allen et al. (2000) are confirmed in Sec. 4.2.4; it is shown, however, that in the limit of small probe radius the difference between the floating potential predicted by OML and that obtained from the full OM theory becomes negligible. Thus the OML result represents the limit of floating potential for small probes, and OML can usually be used for dusty plasmas in spite of the validity criterion.

4.2. Derivation

4.2.1. General equations. The form of derivation follows that of Bernstein and Rabinowitz (1959), with differences in the choice of normalization and modifications to take account of a Maxwellian ion velocity distribution.

The full orbital motion theory involves a description of ion motion at all distances from the probe surface. When (16) is satisfied this theory is compatible with OML. Consider ions around a spherical probe of radius R. We will solve the Vlasov equation (or 'collisionless Boltzmann equation'),

$$\frac{df}{dt} = v \cdot \nabla f - \frac{e}{M} \nabla V \cdot \nabla_v f = 0 \tag{23}$$

and Poisson's equation (19) in the region $R \leqslant r \leqslant \infty$. The electron density is given by (17). For a spherically symmetric, collisionless system we have conservation of ion energy E and angular momentum J, and (23) has the general solution $f(E, J) =$ const.

4.2.2. Ion trajectories and effective potential. Figure 5 shows an ion at distance r from the centre of the probe. The ion has velocity v, comprising a radial component u, and a tangential component w.

Ion density is given by

$$n_{\mathrm{i}}(r) = \int f(v)\, d^3v = \frac{2\pi}{M_{\mathrm{i}}^2 r^2} \int_0^{\infty} \int_0^{J_r} \frac{f(E, J)}{\sqrt{2M_{\mathrm{i}}(E - eV) - (J^2/r^2)}} J\, dJ\, dE. \tag{24}$$

https://doi.org/10.1017/S0022377803002265 Published online by Cambridge University Press

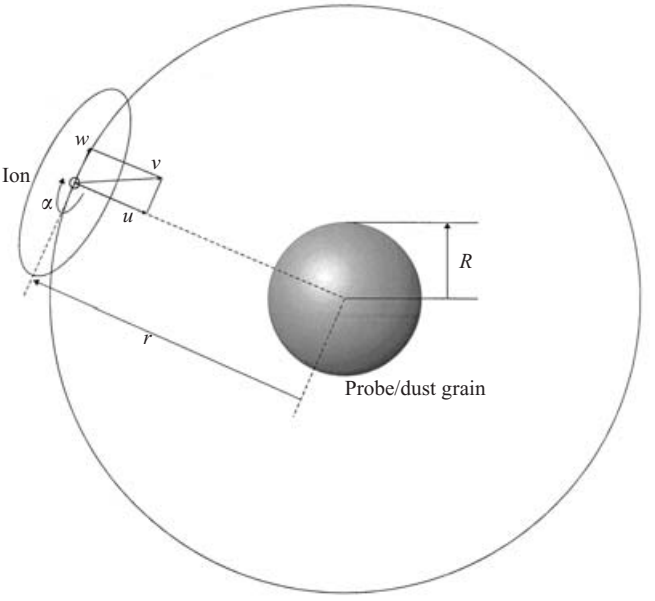

Figure 5. An ion at distance r from the centre of a spherical probe. The ion has velocity v, comprising a radial component u, and a tangential component w.

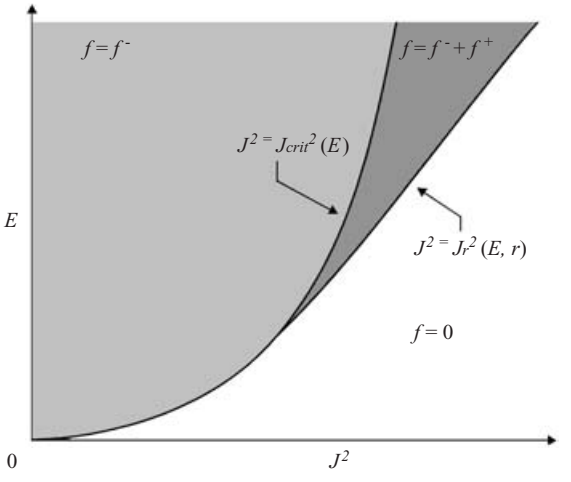

Figure 6. Schematic representation of the space $\{E, J^2\}$ for the integration. The f terms can be found by determining whether an ion of properties $\{E, J\}$ reaches a radius r and whether it will return.

Let

$$f = f^+ + f^- \tag{25}$$

where f^+ represents ions with positive radial velocity (outbound) and f^- ions with negative u (inbound). Figure 6 shows a schematic representation of the space

https://doi.org/10.1017/S0022377803002265 Published online by Cambridge University Press

$\{E, J^2\}$ for the integration. The f terms can be found by determining whether an ion of properties $\{E, J\}$ will:

(a) reach radius r on its way to the surface ($f = f^- = f_{\rm M}$);

(b) reach radius r inbound and outbound ($f = f^+ + f^- = 2f^- = 2f_{\rm M}$ by symmetry);

(c) not reach radius r ($f = 0$).

Which case applies is determined by $J_r(E, r)$ (the largest J at which an ion of energy E can reach r) and $J_{\rm crit}(E)$ (the largest J at which an ion will be absorbed). Note that $J_{\rm crit}(E) = J_r(E, R)$.

Integrating with respect to J,

$$n_{\rm i}(r) = \frac{2\pi}{M_{\rm i}^2} \int_0^\infty f_{\rm M}(E) \Big(\sqrt{2M_{\rm i}(E - eV)}\, dE - \sqrt{2M_{\rm i}(E - eV) - \big(J_{\rm crit}^2(E)/r^2\big)} + 2\sqrt{2M_{\rm i}(E - eV) - \big(J_r^2(E)/r^2\big)} \Big)\, dE. \tag{26}$$

To determine J_r we express (1) in terms of the radial velocity and an effective potential U including angular momentum,

$$E = \tfrac{1}{2} M_{\rm i} u^2 + U(r, J) \tag{27}$$

where the effective potential, from (1) and (27), is

$$U(r, J) = eV(r) + \frac{J^2}{2M_{\rm i}^2 r^2}. \tag{28}$$

When $E = U$, the radial velocity is zero; a particle has reached its minimum radius and is reflected. If there is no maximum of U at larger radius than r, (27) and (28),

$$J_r(E, r) = (J_r)_{\rm OML} = \sqrt{2}\, M_{\rm i} r \sqrt{E - eV(r)}, \tag{29}$$

see Fig. 7(a). We call this $(J_r)_{\rm OML}$ because it is the expression which would apply if OML were valid. However, if there is a maximum of U larger than E at larger radius, the particle will be reflected there, as shown in Fig. 7(b). We define $J^*(E)$ as the angular momentum which gives a peak of U at E. Because U is smooth and monotonic with J, the smallest J for which the ion will be reflected at any radius is J^* where a value exists. When that peak is at a radius larger than r, J_r is given by J^*. Setting the derivative of U to zero, we obtain $\widehat{U}(r)$, the locus of turning points,

$$\widehat{U}(r) = eV(r) + \frac{r}{2} e \frac{dV(r)}{dr}. \tag{30}$$

For J^*, from (27) and (28),

$$J^*(E) = \sqrt{2}\, M_{\rm i} r^*(E) \sqrt{E - eV(r^*)} \tag{31}$$

where r^* is the largest radius for which $\widehat{U} = E$, which will correspond to a maximum of U if the functions are smooth as we can show *a posteriori* that $V(r)$ has a $1/r^2$ form as $r \to \infty$ in the orbital theory, so $\widehat{U}$ tends to zero. Typically, the potential close to a small probe has a vacuum-like $1/r$ form, which gives $\widehat{U} < 0$. Larger probes have a sharper fall near to the surface and may have positive $\widehat{U}$. Figure 8 shows these two general forms of $\widehat{U}$. For the ion density integration (26), there are three

https://doi.org/10.1017/S0022377803002265 Published online by Cambridge University Press

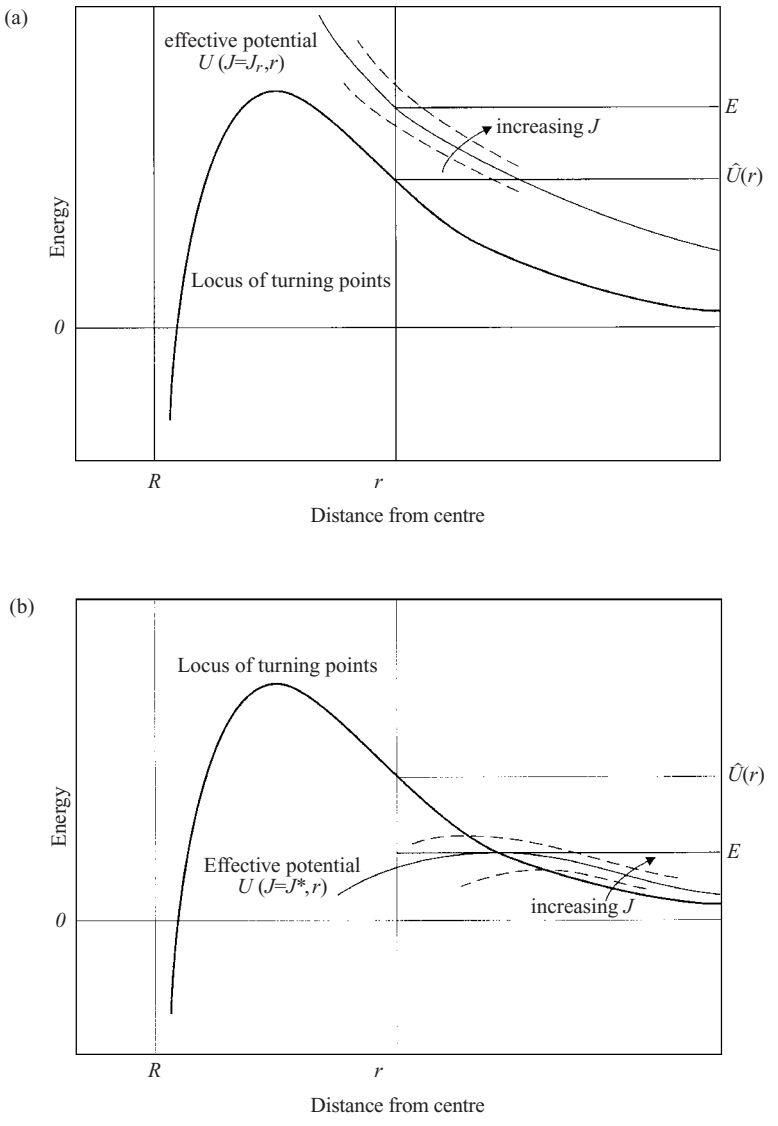

Figure 7. Effective potential energy and the locus of its turning points; the effect of ion energy being larger than or smaller than the turning point at a given radius. (a) E is larger than the turning points, so the largest J an ion can have to reach r is determined by the actual value of the potential at r. (b) E is smaller than a maximum of U which exists at a larger radius than r. The value of J which causes a maximum at E is the largest an ion can have to reach r.

ranges of energy, which we define as follows:

(1) when $E < E_1(r)$, $J_r = J_{\text{crit}} = J^*$;

(2) when $E_1 < E < E_2$, $J_r = (J_r)_{\text{OML}}$ and $J_{\text{crit}} = J^*$;

(3) when $E > E_2$, $J_r = (J_r)_{\text{OML}}$ and $J_{\text{crit}} = \sqrt{2}\, M_{\text{i}} R \sqrt{E - eV_p} = (J_{\text{crit}})_{\text{OML}}$.

https://doi.org/10.1017/S0022377803002265 Published online by Cambridge University Press

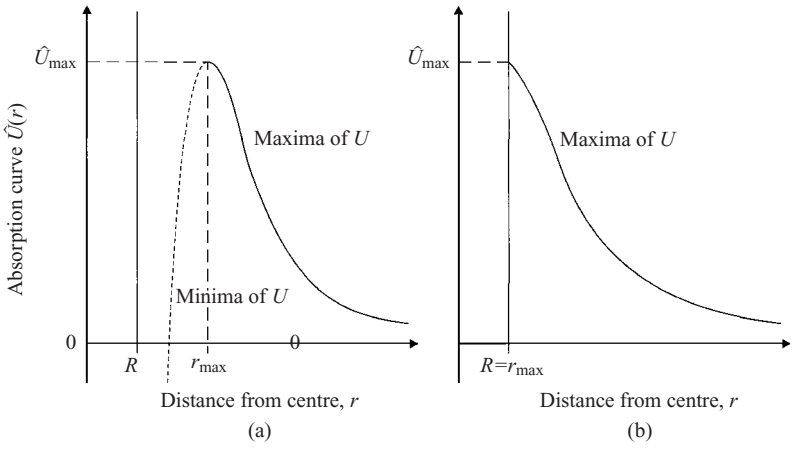

Figure 8. Two general forms of the locus of turning points $\widehat{U}$ of effective potential energy curve U. (a) The maxima exist at r larger than $r_{\max}$; at smaller r only minima exist. (b) Only maxima exist.

Clearly, when $r > r_{\widehat{U}\max}$ we have

$$E_1(r) = \widehat{U}(r). \tag{32}$$

When $r < r_{\widehat{U}\max}$ it is necessary to find the crossover point E_1 by equating $(J_r)_{\mathrm{OML}}$ with J^* at each radius and finding the energy; from (29) and (31) we must solve

$$E_1(r^{*2}(E_1) - r^2) = r^{*2}(E_1)eV(r^*) - r^2 eV(r). \tag{33}$$

Figure 9 shows schematically the relationships between $\widehat{U}(r)$, $eV(r)$, $E_1(r)$, and E_2. Note that E_1 is always larger than the minima on the $\widehat{U}$ curve. As $J_{\mathrm{crit}} = J_r(R)$, by definition

$$E_2 = E_1(R). \tag{34}$$

4.2.3. Ion density. Using our definitions of E_1 and E_2, we divide (26) into three integrals—from zero to E_1, from E_1 to E_2, and from E_2 to infinity. By substituting these definitions and the Maxwellian (10) into (26),

$$N_{\mathrm{i}}(\rho) = \frac{1}{\sqrt{\pi}}\left(\int_0^{\infty} \sqrt{\varepsilon + \phi} + \left(\int_{\varepsilon_1}^{\varepsilon_2} - \int_0^{\varepsilon_1} \right) C(\rho^*) + 2C(P) \right) \exp(-\varepsilon)\, d\varepsilon \tag{35}$$

where we have normalized as follows,

$$N_{\mathrm{i}} = \frac{n_{\mathrm{i}}}{n_0}; \quad \rho = \frac{r}{\lambda_{\mathrm{Di}}}; \quad P = \frac{R}{\lambda_{\mathrm{Di}}}; \quad \varepsilon = \frac{E}{kT_{\mathrm{i}}}; \quad \phi(\rho) = -\frac{eV(r)}{kT_{\mathrm{i}}}; \quad \Phi = \phi(P), \tag{36}$$

and the function C is defined as

$$C(x) = \sqrt{\varepsilon\left(1 - \frac{x^2}{\rho^2}\right) - [\phi(\rho) - \phi(x)]\frac{x^2}{\rho^2}}\,. \tag{37}$$

https://doi.org/10.1017/S0022377803002265 Published online by Cambridge University Press

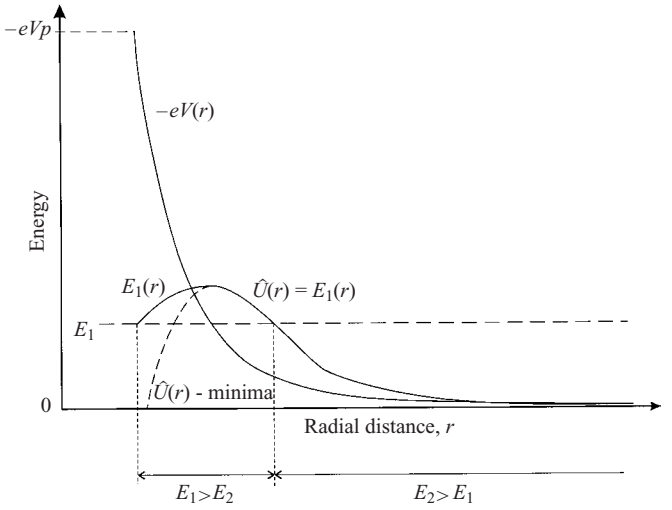

Figure 9. Relationships between the potential energy $eV(r)$, locus of effective potential turning points $\widehat{U}(r)$, absorption curve $E_1(r)$, and critical absorption energy E_2.

Integrating analytically where possible,

$$N_{\mathrm{i}}(\rho) = M(\phi) + \frac{1}{\sqrt{\pi}}\left(\int_{\varepsilon_1}^{\varepsilon_2} - \int_0^{\varepsilon_1}\right) e^{-\varepsilon} C(\rho^*)\, d\varepsilon + \sqrt{1 - \frac{P^2}{\rho^2}}\, e^{\Phi} M\left(\frac{\phi - \Phi(P^2/r^2)}{1 - (P^2/\rho^2)} + \varepsilon_2\right) \tag{38}$$

where the function M is given by

$$M(x) = \sqrt{\frac{x}{\pi}} + \frac{1}{2}\exp(x)(1 - \mathrm{erf}[\sqrt{x}\,]) \tag{39}$$

and erf is the error function, defined as

$$\mathrm{erf}(x) = \frac{1}{\sqrt{\pi}} \int_0^x \exp(-t^2)\, dt. \tag{40}$$

In this normalization, electron density $N_{\mathrm{e}} = n_{\mathrm{e}}/n_0$ is

$$N_{\mathrm{e}}(\rho) = \exp(\beta\phi). \tag{41}$$

Equation (38) expresses the entire ion density in terms of the radius and the potential profile. The absorption radius effects introduce the integral terms in the middle, and cause ε_1 and ε_2 to be non-zero, where $\varepsilon_1(\rho) = E_1(r)/kT_{\mathrm{i}}$ and $\varepsilon_2 = E_2/kT_{\mathrm{i}}$. Define the normalized locus of turning points as $\widehat{v} = \widehat{U}/kT_{\mathrm{i}}$. From (30),

$$\widehat{v}(\rho) = -\phi(\rho) - \frac{\rho}{2}\frac{d\phi}{d\rho} \tag{42}$$

https://doi.org/10.1017/S0022377803002265 Published online by Cambridge University Press

and the limits of energy integration are, from (32)–(34),

$$\varepsilon_1(\rho) = \begin{cases} \varepsilon \ni \dfrac{(\rho^{*2}-\rho^2)\varepsilon}{\rho^{*2}\phi^* - \rho^2\phi} = 1 & \rho < \rho(\widehat{v}_{\max}) \\ \widehat{v}(\rho) & \rho > \rho(\widehat{v}_{\max}) \end{cases} \tag{43}$$

$$\varepsilon_2 = \varepsilon_1(R). \tag{44}$$

where $\rho^* = \rho \ni \widehat{v}(\rho) = \varepsilon$ and $\phi^* = \phi(\rho^*)$.

4.2.4. The plasma solution. Far enough into a plasma from any solid surface, it is expected that quasi-neutrality will apply, i.e. the electron and ion densities will be approximately equal. Applying this condition in the present theory, and linearizing for small potential, (38) and (41) give

$$\phi(\rho) = \frac{1}{2(1+\beta)}\left(e^{-\varepsilon_2}M(\varepsilon_2) + \Phi(1-\operatorname{erf}\sqrt{\varepsilon_2}) + \frac{1}{\sqrt{\pi}}\int_0^{\varepsilon_2} e^{-\varepsilon}\frac{\rho^2}{\rho^{*2}}\frac{\phi^*+\varepsilon}{\varepsilon^{1/2}}\,d\varepsilon\right)\frac{P^2}{\rho^2}. \tag{45}$$

Setting ε_2 to zero gives the expression

$$\phi(\rho) = \frac{1+2\Phi}{4(1+\beta)}\frac{P^2}{\rho^2}. \tag{46}$$

The OML solution for Φ in the ion normalization is, from (13),

$$(1+\Phi)\exp(\beta\Phi) = \sqrt{\frac{M_{\rm i}}{m_{\rm e}}}\sqrt{\beta} \tag{47}$$

and it is found that using Φ from (47) in (46) violates the condition (16) for all reasonable values of $M_{\rm i}$, and

$$\beta : \frac{V(r)}{V_p} > \frac{R^2}{r^2}.$$

Thus Allen et al. (2000) concluded that the use of OML was questionable for dusty plasma applications.

4.2.5. Ion current. The ion current $I_{\rm i}$ is given by integrating the inbound flux over the velocities:

$$I_{\rm i} = 4\pi R^2 \int_{u<0} f(v) e u(R)\, d^3v. \tag{48}$$

Substituting (8) for d^3v,

$$I_{\rm i} = \frac{8\pi^2 e}{M_{\rm i}^2}\int_0^\infty \int_0^{J_{\rm crit}} f^-(E) J\, dJ\, dE. \tag{49}$$

Integrating with respect to J and substituting (5) and (31) for $J_{\rm crit}$,

$$I_{\rm i} = \frac{8\pi^2 e}{M_{\rm i}^2}\left[\int_0^{E_2} f_{\rm M} r^{*2}(E - eV[r^*])\, dE + \int_{E_2}^\infty f_{\rm M} R^2 (E - eV_p)\, dE\right]. \tag{50}$$

Substituting (10) for $f_{\rm M}$, the second integral is analytical. Normalizing for current using $i_{\rm i} = I_{\rm i}/(4\pi\lambda_{\rm Di}^2 n_0 e\sqrt{2kT_{\rm i}/M_{\rm i}})$,

$$i_{\rm i} = \frac{P^2(1+\Phi)}{2\sqrt{\pi}} - \frac{1}{2\sqrt{\pi}}\int_0^{\varepsilon_2} e^{-\varepsilon}[P^2(\varepsilon+\Phi) - \rho^{*2}(\varepsilon + \phi[\rho^*])]\, d\varepsilon. \tag{51}$$

https://doi.org/10.1017/S0022377803002265 Published online by Cambridge University Press

The first term in (51) is the OML current, see (11). In the case of $\varepsilon_2 \to 0$ we recover this current (assuming the integrand remains finite), and hence the floating potential. The integrand in the second term is always positive.

RESULT. *For any solution of the full orbital system, the ion current for a given floating potential is always less than or equal to the OML ion current.*

COROLLARY. *Floating potential in the full orbital system is always greater than or equal to the OML floating potential.*

From a physical point of view any ion which approaches the surface—having passed any absorption radii along the way—must still satisfy the condition of having a small enough angular momentum. A potential distribution that produces absorption radii can prevent some ions from getting far enough to meet that test, but cannot increase the number of ions that reach the surface.

4.2.6. Solving for the potential profile. To obtain the potential distribution around a sphere of known surface potential, we must solve the Poisson equation, (19), with electron and ion density from (17) and (38), respectively. Normalizing (19) and substituting (17) and (38),

$$\frac{d^2\phi}{d\rho^2} + \frac{1}{\rho}\frac{d\phi}{d\rho} = M(\phi) + \frac{1}{\sqrt{\pi}}\left(\int_{\varepsilon_1}^{\varepsilon_2} - \int_0^{\varepsilon_1}\right) e^{-\varepsilon}\sqrt{\varepsilon\left(1-\frac{\chi}{\chi^*}\right) + \left(\phi - \phi^*\frac{\chi}{\chi^*}\right)}\, d\varepsilon + \sqrt{1-\chi}\, e^{-\varepsilon_2}\left[M(\varepsilon_2) + \frac{1}{2}e^{\varepsilon_2}(1-\operatorname{erf}\varepsilon_2)(\phi - \Phi\chi)\right] - \exp(-\beta\phi). \tag{52}$$

Once this is done, we may find the electron and ion currents to the surface, and adjust the surface potential accordingly to find the floating potential. When ARs exist, (38) and (52) are functions of the entire potential profile, so an iterative solution is required. It has been found that a point-and-shoot method works well—we integrate from the surface outwards to a sufficiently large radius, varying the initial slope of the potential until the curve meets the plasma solution, (45). A new program was written to calculate the potential in full—which has not been done since Laframboise's work (1966). That work did not contain many results for small probes or at floating potential.

4.2.7. Results

Floating potential. Results were obtained for a range of β from 0.01 to 1 and a range of radii from 0.001 to $10\lambda_{De}$. Although it is much more convenient to express (52) in terms of ion normalized values, results are better shown electron-normalized, because electron temperature is much easier to measure. Let

$$\xi = \frac{r}{\lambda_{De}}; \quad \Xi = \frac{R}{\lambda_{De}}; \quad \eta(\xi) = -\frac{eV(r)}{kT_e}; \quad \eta_p = \eta(\Xi). \tag{53}$$

Figure 10 shows the electron-normalized floating potential as a function of probe radius. For each temperature, the potential increases with radius. There is a finite

https://doi.org/10.1017/S0022377803002265 Published online by Cambridge University Press

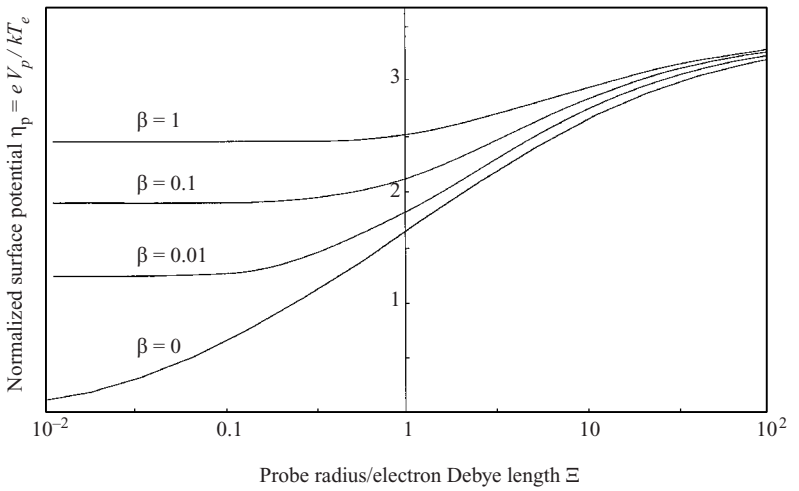

Figure 10. The electron-normalized floating potential as a function of probe radius for various ratios of ion to electron temperature β. Results are due to the full OM theory, except for those for $\beta = 0$, which are obtained from the radial motion theory (Kennedy and Allen 2001). For each temperature ratio, the potential increases with radius. There is a finite asymptote for small probes which corresponds to the OML potential.

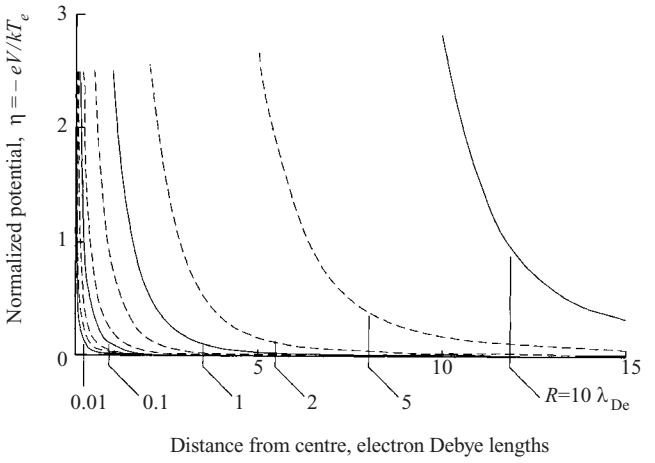

Figure 11. Potential profiles for spherical probes at floating potential from the full orbital theory, at various ratios of probe radius to Debye length, where ion and electron temperature are equal.

asymptote for small probes which corresponds to the OML potential, a new result which is demonstrated in the following section.

Potential profiles. Figure 11 shows potential profiles for spherical probes at floating potential from the full orbital theory. It is apparent that the profile becomes sharper as probe radius decreases, as it did in the radial model. In order to expose the underlying properties of these potential curves we plot them on a logarithmic scale. Figure 12 shows a logarithmic plot, with potential scaled by the relevant floating

https://doi.org/10.1017/S0022377803002265 Published online by Cambridge University Press

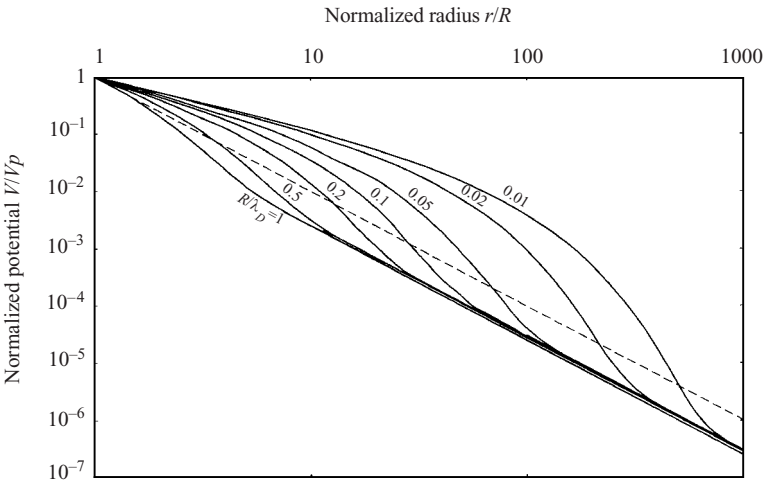

Figure 12. Logarithmic plot of the results shown in Fig. 10, with potential scaled by the relevant floating potential and radius scaled by the probe radius. There is usually a vacuum-like region near the surface where the slope is approximately −1. Far from the probe, the plasma region has a slope of −2.

potential and radius scaled by the probe radius. In general, there is a vacuum-like region near the surface where the slope is approximately −1. Far from the probe, the plasma region has a slope of −2, although this asymptote shifts with R/λ_{De}. In between there is a transition region, in which the curve crosses the dashed OML criterion line through the origin of slope −2. The fact that each potential curve passes beneath this line means that each of these solutions has a finite absorption radius for some range of energies.

Variation with probe radius. Laframboise (1966) gives results of spatial potential and density distribution, ion and electron current for ion and electron temperature ratios varying from 0.1 to unity, but rarely for $R/\lambda_{\mathrm{D}} < 1$, and never for R/λ_{D} less than 0.2. His results were not at floating potential but were specified for various potentials, often larger than $10kT_{\mathrm{e}}$. Hence the student of dust will not generally use these results except as a guide for the accuracy of a calculation mechanism.

Looking at a large probe, as in Fig. 13, we see that within a few probe radii, the ion and electron densities are approximately equal, and the transition between the effective sheath and pre-sheath occurs at around $eV = -\frac{1}{2}kT_{\mathrm{e}}$. The absorption curve ε_1 is very prominent here, having significant values well beyond the sheath boundary. The Maxwellian, drawn for comparison, is shown to the same scale; almost all the ions in the distribution have an absorption radius. The largest value of ε_1 in this case is 42.3, and it occurs at the probe surface, so $\varepsilon_2 = \widehat{v}_{\max}$. The surface potential is $\eta_p = 3.182$, which is close to the thin-sheath limit.

A probe an order of magnitude smaller, with $R/\lambda_{\mathrm{D}} = 10$, has similar characteristics, but at a different distance scale, as shown in Fig. 14. The surface potential is somewhat smaller, at 2.815, and $\widehat{v}_{\max}$ is only 4.66. It is still an absorption radius-dominated system however; most ions in the Maxwellian spectrum have an absorption radius.

https://doi.org/10.1017/S0022377803002265 Published online by Cambridge University Press

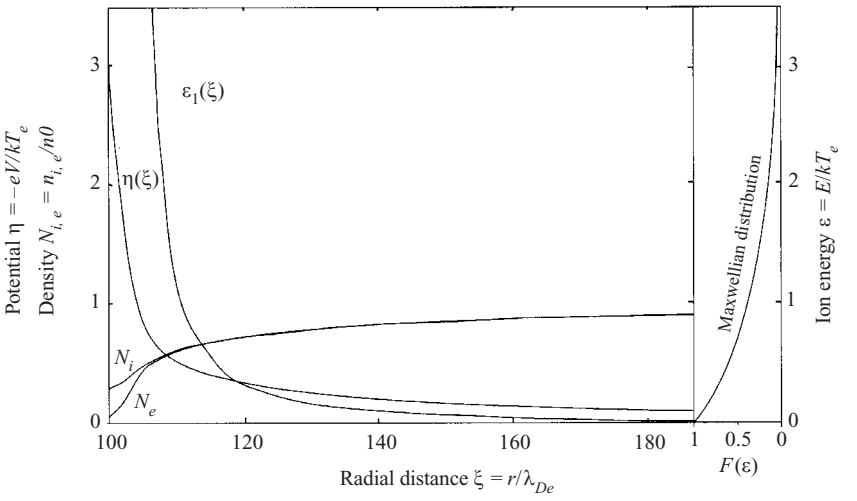

Figure 13. Surface potential, absorption curve, and ion and electron charge densities N_i and N_e. $T_\mathrm{i}/T_\mathrm{e} = 1$; $R/\lambda_\mathrm{D} = 100$.

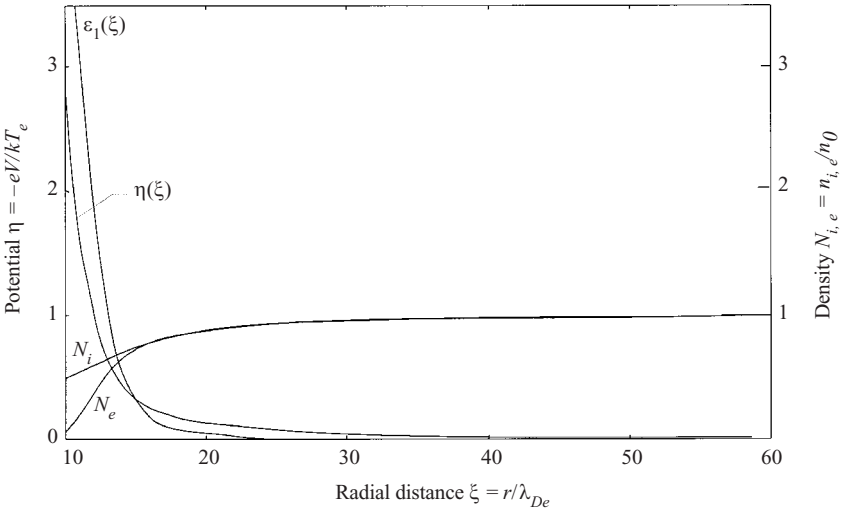

Figure 14. Surface potential, absorption curve, and ion and electron charge densities N_i and N_e. $T_\mathrm{i}/T_\mathrm{e} = 1$; $R/\lambda_\mathrm{D} = 10$.

With a probe which has $R/\lambda_\mathrm{D} = 1$—shown in Fig. 15—the absorption curve has changed shape. Now it has a peak, which means that the absorption radii start some way from the surface. Much less of the ion distribution is affected by this curve. Also, the plasma region now starts at around $r = 5R$; the sheath is becoming large compared to the probe radius. The surface potential for this radius is 2.52, very close to the OML value.

With a probe of $R/\lambda_\mathrm{D} = 0.1$—shown in Fig. 16—we start to approach the dust regime, and the limit of Laframboise's results. Now the absorption curve cannot be clearly seen on the same scale as the potential. The peak has moved much

https://doi.org/10.1017/S0022377803002265 Published online by Cambridge University Press

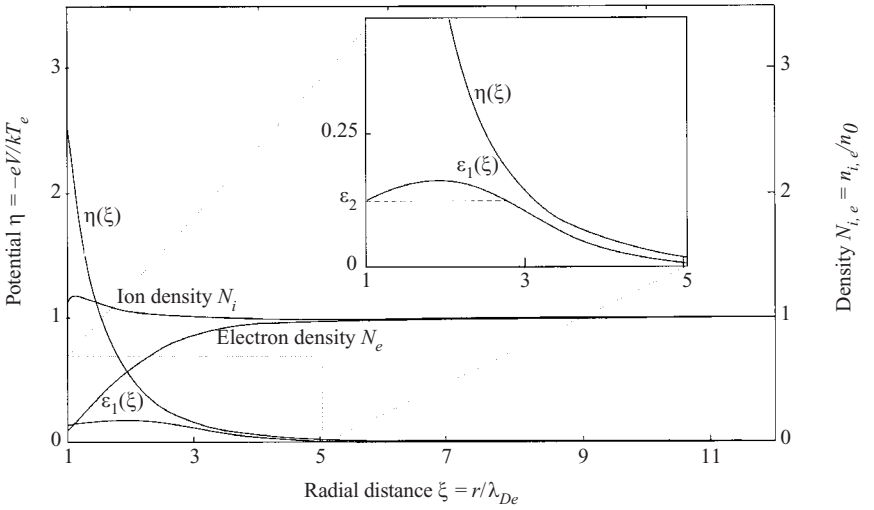

Figure 15. Surface potential, absorption curve, and ion and electron charge densities N_i and N_e. $T_\mathrm{i}/T_\mathrm{e} = 1$; $R/\lambda_\mathrm{D} = 1$.

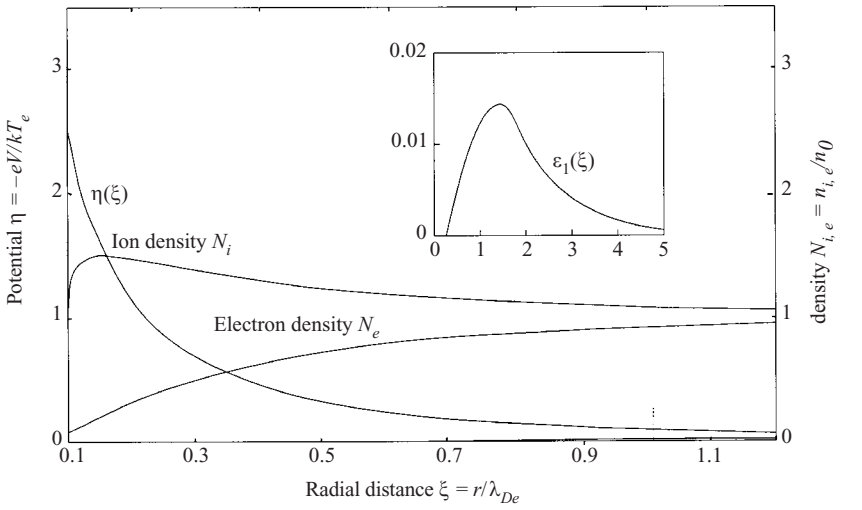

Figure 16. Surface potential, absorption curve, and ion and electron charge densities N_i and N_e. $T_\mathrm{i}/T_\mathrm{e} = 1$; $R/\lambda_\mathrm{D} = 0.1$.

further out, and to fully encompass all of the absorption behaviour we must look at positions many times larger than the probe radius. This has little effect on floating potential however, which is now 2.505.

Finally, at $R/\lambda_\mathrm{D} = 0.01$—shown in Fig. 17—we completely lose sight of the absorption curve on the scale of the potential. Here, ε_1 has little effect on the ion density or the potential. Empirically it appears that absorption radii have little effect for these parameters. We recover the OML floating potential $\eta_p = 2.503$ (see Sec. 5).

https://doi.org/10.1017/S0022377803002265 Published online by Cambridge University Press

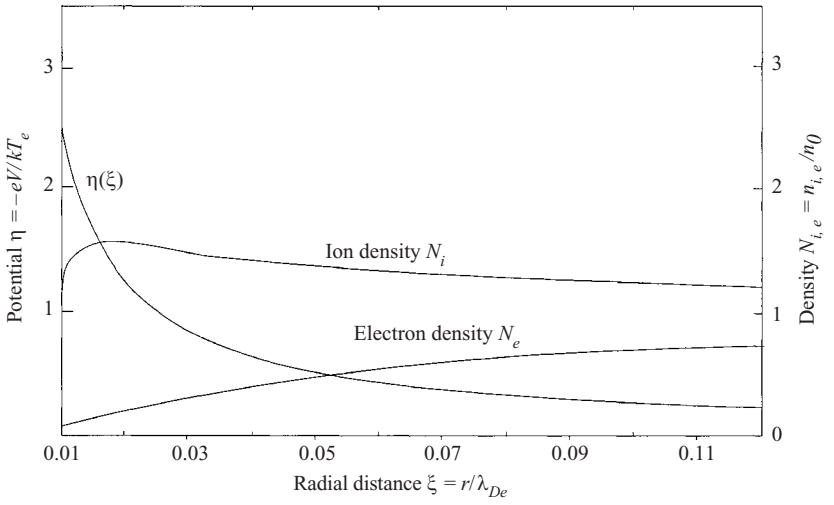

Figure 17. Surface potential, absorption curve, and ion and electron charge densities N_i and N_e. $T_\mathrm{i}/T_\mathrm{e} = 1$; $R/\lambda_\mathrm{D} = 0.01$.

Variation with ion–electron temperature ratio. Figure 18 shows three potential curves which demonstrate the variation of the theoretical results with temperature ratio β. As β is reduced, the floating potential decreases, also shown in Fig. 18. The potential curve becomes steeper as β decreases; the system is becoming more influenced by absorption radius effects. The absorption curve ε_1 increases in magnitude due to this steepening. The extreme case is that of zero ion temperature, which cannot be solved using this method. Effectively in this case, every ion which approaches the probe has an absorption radius at infinity, and all linearizations of ion-normalized energies become untenable, involving a division by zero. Hence in this case we change the calculation method completely and use the radial motion theory. Generally as β is reduced the calculation becomes slower and more difficult to control.

5. Limiting theory of small probe radius

5.1. Linear theory and solution

In Sec. 4.2.4 it was shown that as ε_2 goes to zero we recover the OML expressions for the ion current and surface potential. Here it will be shown that ε_2 diminishes with the ratio of probe radius to Debye length.

Taking (52), and eliminating terms above first order in $1/\rho^2$ (we will use ζ for consistency) and ϕ, assuming also that the integral term is negligibly small (to be confirmed *a posteriori*),

$$\frac{d^2\phi}{d\zeta^2} + \frac{1}{\zeta}\frac{d\phi}{d\zeta} = \phi - \frac{1+2\Phi}{4}\frac{Z^2}{\zeta^2}. \tag{54}$$

Compare (54) to the Debye–Hückel equation, (20), which lacks the latter term of the charge density. This term, $-(1+2\Phi)Z^2/(4\zeta^2)$ represents the ion deficit due to absorption on the probe surface, which is neglected in the Debye–Hückel analysis.

https://doi.org/10.1017/S0022377803002265 Published online by Cambridge University Press

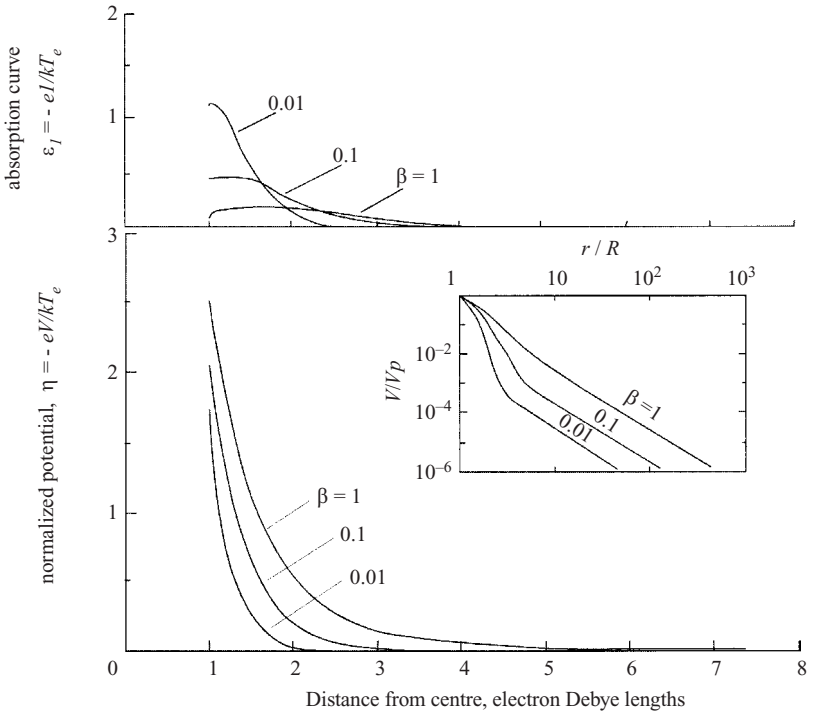

Figure 18. Results from full orbital motion theory. The potential η and absorption curve ε_1 as a function of radial distance for various values of $\beta = T_i/T_e$, and $R/\lambda_{De} = 1$. A logarithmic plot of potential is shown in the inset.

Equation (54) has the *analytical* solution,

$$\phi = e^{Z-\zeta}\frac{Z}{\zeta}\Phi + \frac{1+2\Phi}{8(1+\beta)}\frac{Z^2}{\zeta}e^{-\zeta}(e^{\zeta}f(\zeta) - e^{Z}f(Z)) \tag{55}$$

where we have used a distance-normalization based on the linearized Debye length λ_L, so that $\zeta = r/\lambda_{DL}$ and $Z = R/\lambda_{DL}$. Note that $e^x f(x)$ is monotonic, therefore the latter term in (55) is always positive and ϕ is always larger than the Debye–Hückel solution. The function f is defined as

$$f(x) = e^{-x}\,\mathrm{Ei}(x) - e^{x}\,\mathrm{Ei}(-x)$$

where Ei is the exponential integral function,

$$\mathrm{Ei}(x) = -\int_{-z}^{\infty}\frac{e^{-t}}{t}\,dt. \tag{56}$$

Figure 19 shows a potential plot from (55) compared to the Debye–Hückel solution and the full solution for the same surface potential. The linear theory gives an excellent fit to the full solution at small radius. The difference lies in the inverse square behaviour at larger radius, which is reproduced accurately by the new model, whereas the Debye–Hückel potential vanishes exponentially. The argument of Sec. 3 still applies—the linearization is correct at small potential, and irrelevant at larger potential provided that most of the potential follows a vacuum-like inverse power curve.

https://doi.org/10.1017/S0022377803002265 Published online by Cambridge University Press

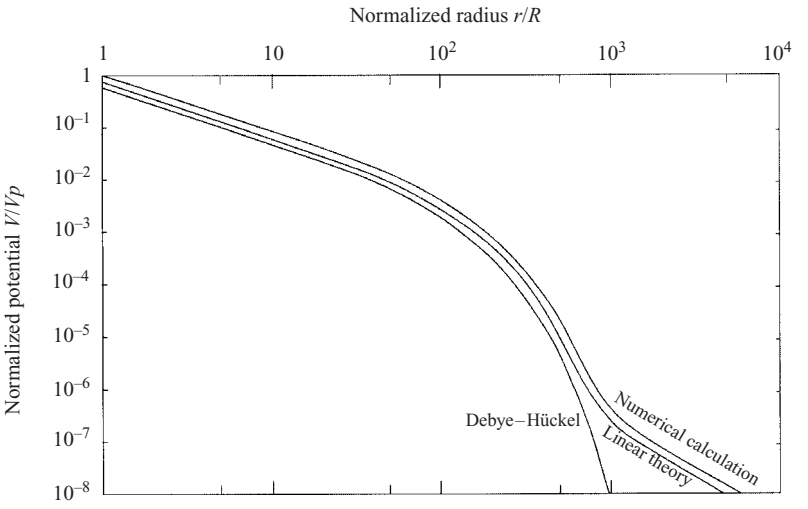

Figure 19. The potential distribution around a spherical probe of radius $R = 10^{-3}\lambda_{De}$. The full orbital results are shown together with the results of the Debye–Hückel model and the new linear theory.

5.2. Absorption radius in the small probe limit

Now compare (52) to (54). Aside from the linearization, the difference is that the integral term must be neglected. In order to do this, ε_2 and ε_1 must vanish as P tends to zero. Consider the effective potential locus of extrema $\widehat{v} = \widehat{U}/kT_i$. From (30),

$$\widehat{v}(\rho) = -\phi - \frac{\rho}{2}\phi'(\rho). \tag{57}$$

Substituting (55) into (57),

$$\widehat{v}(\zeta) = \frac{1}{2}\frac{Z}{\zeta}\left(e^{Z-\zeta}(\zeta-1)\Phi - Z\frac{1+2\Phi}{8(1+\beta)}(f(\zeta)+\zeta g(\zeta)+(\zeta-1)e^{Z-\zeta}f(Z))\right). \tag{58}$$

We seek the maximum of (58). In the limit of small Z, (58) reduces to

$$\widehat{v}(\zeta) = \frac{1}{2}\frac{Z}{\zeta}e^{Z-\zeta}(\zeta-1)\Phi \tag{59}$$

which is also the expression when the Debye–Hückel potential applies. Equation (59) has an analytical maximum $\widehat{v}_{max}$ at $\zeta = 1.618\,03$ equal to $0.037\,87Z\Phi$, which of course reduces to zero as P or Z tends to zero. As ε_2 must be less than this maximum, we have shown that ε_2 reduces to zero as $Z \to 0$. All values of ε_1 are less than $\widehat{v}_{max}$, so the entire integral in (52) becomes negligible (the integrand can be shown to remain finite). Furthermore, (51) reduces to the OML current of (11) as ε_2 vanishes, so we obtain the OML potential in the limit of small probe radius.

6. Conclusions

Calculations have been performed for the full orbital theory with a Maxwellian ion distribution, showing clearly the form of the potential, densities, and absorption curve for various parameters. It has been shown from first principles that the

https://doi.org/10.1017/S0022377803002265 Published online by Cambridge University Press

OML surface potential is the limiting solution to the complete orbital motion theory for vanishing probe radius divided by any appropriate Debye length. An analytical solution has been given which applies in this limit. Both of these results are pertinent to dusty plasma applications, wherein R/λ_D is usually expected to be small compared to unity.

This analysis assumes that ion motion is collisionless. It may also be that collisions have the effect of depleting ion angular momentum, thus increasing the ion current, and reducing the equilibrium potential. Collisions may also lead to ions becoming trapped in closed orbits around the dust grain, when the effective potential has a local maximum (see, for example, Goree 1994).

Considering the calculated surface potentials, it is clear that even a small ion temperature gives rise to a significantly larger potential than is predicted by radial motion theory (see Kennedy and Allen 2001). This difference increases as probe size becomes smaller. In the case of dust it seems that, of the theories considered, the orbital theory, either in full or simplified, is most appropriate for dusty plasma work.

References

Allen, J. E., Annaratone, B. M. and de Angelis, U. 2000 On the orbital motion limited theory for a small body at floating potential in a Maxwellian plasma. *J. Plasma Phys.* **63**, 299–309.

Allen, J. E., Boyd, R. L. F. and Reynolds, P. 1957 The collection of positive ions by a probe immersed in a plasma. *Proc. Phys. Soc.* B **70**, 297–304.

Al'Pert, Ya. L., Gurevich, A. V. and Pitaevskii, L. P. 1995 *Space Physics with Artificial Satellites*, English edn. New York: Plenum Press.

Bernstein, I. B. and Rabinowitz, I. M. 1959 Theory of electrostatic probes in a low-density plasma. *Phys. Fluids* **2**, 112–121.

Bohm, D., Burhop, E. H. S. and Massey, H. S. W. 1949 The use of probes for plasma exploration in strong magnetic fields. In: *The Characteristics of Electrical Discharges in Magnetic Fields* (ed. A. Guthrie and R. K. Wakerling). New York: McGraw-Hill, pp. 13–76.

Bouchoule, A. (ed.) 1999 *Dusty Plasmas*. New York: John Wiley & Sons, p. 366.

Chen, F. F. 1965 Numerical computations for ion probe characteristics in a collisionless plasma. *J. Nucl. Energy C: Plasma Phys.* **7**, 47–67.

Goree, J. 1994 Charging of particles in a plasma. *Plasma Sources Sci. Technol.* **3**, 400–406.

Daugherty, J. E., Porteous, R. K., Kilgore, M. D. and Graves, D. B. 1992 Sheath structure around particles in low-pressure discharges. *J. Appl. Phys.* **72**(9), 3934–3942.

Kennedy, R. V. and Allen, J. E. 2001 The floating potential of spherical probes and dust grains. I: Radial motion theory. *J. Plasma Phys.* (submitted).

Laframboise, J. G. 1966 The theory of spherical and cylindrical probes in a collisionless, Maxwellian plasma at rest. Report 100, Institute for Aerospace Studies, University of Toronto (UTIAS).

Mott-Smith, H. M. and Langmuir, I. 1926 The theory of collectors in gaseous discharges. *Phys. Rev.* **28**, 727.

Nowlin, R. N. and Carlile, R. N. 1991 The electrostatic nature of contaminative particles in a semiconductor processing plasma'. *J. Vacuum Sci. Technol.* A **9**(5), 2825–2833.